This is the peer reviewd version of the followng article:

A simulation study of FET-based nanoelectrodes for active intracellular neural recordings / Leva, Federico; Palestri, Pierpaolo; Selmi, Luca. - In: PROCEEDINGS OF THE ... IEEE CONFERENCE ON NANOTECHNOLOGY. - ISSN 1944-9399. - 2022-:(2022), pp. 279-282. (2022 IEEE 22nd International Conference on Nanotechnology (NANO) Palma de Mallorca July, 4-8 2022) [10.1109/NANO54668.2022.9928642].

IEEE Computer Society
Terms of use:

The terms and conditions for the reuse of this version of the manuscript are specified in the publishing policy. For all terms of use and more information see the publisher's website.

02/05/2026 02:51

(Article begins on next page)

© 20XX IEEE. Personal use of this material is permitted. Permission from IEEE must be obtained for all other uses, in any current or future media, including reprinting/ republishing this material for advertising or promotional purposes, creating new collective works, for resale or redistribution to servers or lists, or reuse of any copyrighted component of this work in other works.

A simulation study of FET-based nanoelectrodes for active intracellular neural recordings

Federico Leva
Dipartimento di Ingegneria Enzo Ferrari
University of Modena and Reggio Emilia
Modena, Italy
federico.leva@unimore.it

Pierpaolo Palestri
Polytechnic department of Engineering and Architecture, University of Udine
Udine, Italy
pierpaolo.palestri@uniud.it

Luca Selmi
Dipartimento di Ingegneria Enzo Ferrari
University of Modena and Reggio Emilia
Modena, Italy
luca.selmi@unimore.it

***Abstract*—Active FET-based nanoelectrodes are promising candidates to serve as sensors for neural signal recording. Based on a multiscale-multiphysics TCAD modelling framework, we study the interaction of two representative nanoelectrode architectures in intracellular contact with neurons. The methodology is explained, and DC, AC, and transient simulations are extensively used to compare the main performance metrics of the proposed structures. The lateral coating of the nanoelectrode results to be a key-parameter to control the sensor performance.**

***Index Terms*—neural recording, intracellular sensing, TCAD, modelling, Hodgkin-Huxley**

I. Introduction

In-vitro and *in-vivo* neuroscience studies to better understand neural-network working principles, experiment the treatment of neurological disorders, and develop reliable and stable human-brain interfaces [1], [2], require advanced neural sensors featuring high spatio-temporal resolution, long-term recording, and sensitivity to sub- and supra-threshold potentials with high signal-to-noise ratio (SNR) [3]. Only miniaturized electrodes can achieve high spatial-resolution of one or more electrodes per neuron while fostering intracellular access [4] for enhanced sensitivity to subthreshold signals compared to less invasive extracellular electrodes. However, the reduced contact area increases the nanoelectrode impedance and degrades the SNR, making passive electrodes unsuitable to convey the tiny bio-signals via long interconnects. Instead, active field-effect-transistor (FET)-based sensors integrated in the front-end-of-line (FEOL) or back-end-of-line (BEOL) of complementary-metal-oxide-semiconductor (CMOS) fabrication processes can amplify the signal *in-situ*, effectively drive (long) interconnects, and overcome most of the electrode miniaturization drawbacks. Improving the design of such devices requires technology-CAD (TCAD) and multiscale-multiphysics simulation platforms (e.g, [5], [6]) to realistically estimate the sensor performance prior to device fabrication and experiments, thus speeding-up the design flow while saving fabrication time and costs.

In previous works [7] we developed a simulation methodology to study sensing devices coupled to neurons. Here we extend such method to compare two active device architectures in intracellular contact with neurons. Sect. II recaps our TCAD-based methodology [7] and describes its extensions in this work. Sect. III presents the devices under study. Sect. IV investigates their performance in terms of threshold-voltage adjustment, transient response to action potentials (APs), and linear transfer functions. Conclusions are given in Sect. V.

This work has been financially supported by the European Union's Horizon-2020 project "IN-FET" (Grant Agreement n. 862882).

II. Methodology

A special simulation deck has been set up to describe the neuron/active electrode interaction with a commercial TCAD tool for semiconductors integrating mixed-mode device-circuit simulation capabilities. The essential physics of the electrolyte is modelled as in [7]–[9] and inherently comprises the formation of electrical double layers (EDLs) at charged surfaces.

The cellular membrane is described either as a lossless insulator directly in the TCAD domain compartment [7] with a relative permittivity $\varepsilon_{r,memb} \approx 11$, and a capacitance $C_m \approx 1$ $\mu F/cm^2$ consistent to those of neurons [10], or as a lumped capacitor for any non-TCAD domain compartment. To elicit action potentials (APs) onto each membrane's compartment we employ the time-invariant version of the Hodgkin-Huxley (HH) circuit model [11], similarly to [12], [13]. By default, the TCAD only handles circuits with conventional electrical components (resistor, capacitor, diode, etc.) described by netlists and solved together with the discretized physical domain. To include custom multi-port components (e.g., the non-linear time-invariant memristive dipoles in the HH [11]), we use the TCAD compact model interface (CMI, [5]). The CMIs set the activation/deactivation state-variables (i.e., n, m, and h [14]) for the non-linear conductances of the K^+ and Na^+ ion-channels of the HH [12], [13]. Their characteristic curves in the left panels of Fig. 1 come from the representative one-compartment HH circuit in Fig. 1 (right panel) that includes a constant conductance for the leakage transmembrane current, and three voltage sources as reversal-potentials for the ions. The area (A) of each compartment is a parameter of the HH circuit model and the related membrane representing that compartment. In this work we used only two compartments [15], [16]: one represents the *intrinsic* portion of the membrane included in the TCAD numerical simulation domain and intimately interacting with the device; the other one represents the remaining *extrinsic* portion of the neuron membrane. The

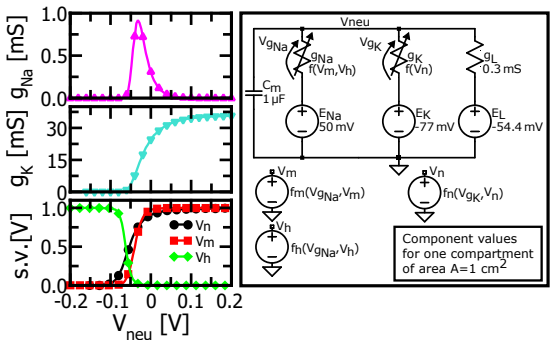

Fig. 1. Na^+ (top-left panel), K^+ (middle-left panel) ion channel conductance and state variables (s.v., bottom-left panel) versus intracellular potential V_{neu} for a representative one-compartment HH circuit with A=1 cm^2 (right panel). C_m is the membrane capacitance, g_K and g_{Na} are the non-linear conductances of the K^+ and Na^+ ions; g_L is the constant conductance for the transmembrane leakage current; E_{Na}, E_K, E_L are the reversal-potentials for the ions. Following [12], [13], the dimensionless n, m, h state variables take the form of voltage sources V_n, V_m, V_h. Their behaviour is defined by the f_n, f_m, f_h equations of the HH [14] needed to control the voltage-dependent $g_K=f(V_n)$ and $g_{Na}=f(V_m, V_h)$.

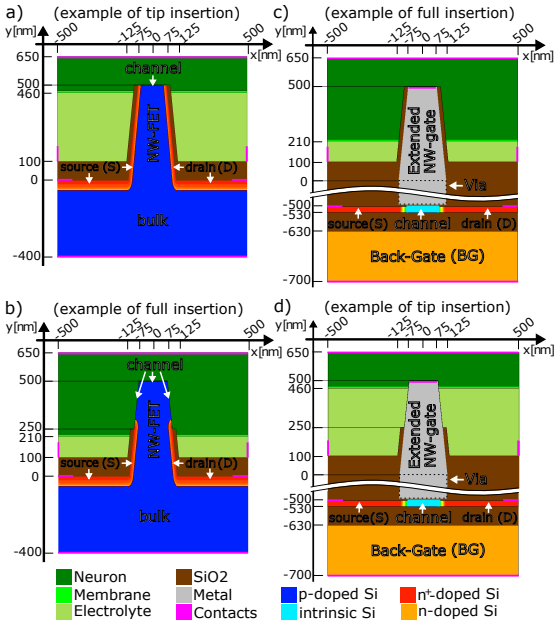

Fig. 2. 2D representation of: (a, b) *vertical NW-FET* (VNW-FET) with a portion of the channel penetrating the neuron; (c, d) *extended-gate silicon-on-insulator FET* (EG-SOI-FET) with the top metallic nanoelectrode in intracellular contact with a neuron. W=150 nm in z-direction. Tab. I lists the region's physical parameters. Each structure has two possible implementations: (a, c) NW fully coated by the lateral dielectric; (b, d) NW partially coated by the lateral dielectric. For each device we consider: (b, c) full insertion of the nanoelectrode in the neuron; (a, d) insertion of the tip only.

respective areas (A_{int} and A_{ext}) are reported in Tab. I and are consistent with those of small neurons [17].

The sensors are built of default TCAD materials (e.g., Silicon, SiO_2, Metals). All mobility degradation models are included in the drift-diffusion transport simulations.

III. Device Description

Fig. 2 reports the structures, sizes, materials and region names of two promising solutions for active intracellular neural sensing envisioned in this work; namely: 1) *vertical nanowire-FET* (VNW-FET) with a portion of the channel penetrating into a neuron (a and b); 2) *extended-gate silicon-on-insulator FET* (EG-SOI-FET) with the top gate (a metallic NW) in intracellular contact (c and d). Physical and geometrical parameters used in simulations are listed in Tab. I.

The VNW-FET can be fabricated in the FEOL, e.g., by etching the outer parts of a Silicon fin and source/drain solid state diffusion from a patterned highly doped dielectric-layer. The EG-SOI-FET is a SOI transistor whose front-gate is extended up to the top metal-layer and exposed to the electrolyte and neurons. The exposed electrode is thus fabricated in the CMOS BEOL.

The structures are solved in rectangular coordinates; the chosen W=150 nm makes the top-most tip tiny enough to pierce the cell membrane [4]. Each structure comes with a lateral oxide fully (a, c) or partially (b, d) coating the nanoelectrode. For all structures we consider intracellular access by insertion of the *tip* only (Fig. 2 a, d) or the *full* nanoelectrode (Fig. 2 b, c).

The devices' working principle resembles that of a conventional MOSFET, except that gate control is exerted by the intracellular potential of the neuron coupled to the active device via the VNW body or the extended FET gate. Modulation of the intracellular potential is then translated into drain current (I_D) changes at V_{DS} = 50 mV.

IV. Results

A. FET's threshold voltage adjustment

To deliver high sensitivity, the FET threshold voltage (V_T) has to be adjusted in order to locate the peak-transconductance ($g_{m,MAX}$) in the middle of the typical AP voltage range (-90 ÷ 40 mV), that is $V_{neu,m}$=-25 mV. An approximately constant g_m over the AP voltage range also yields small non-linear distortion of the transduced AP signals. Threshold voltage modulation can be achieved by jointly applying: 1) a voltage V_{bias} to the bulk, source and drain contacts of the VNW-FET

TABLE I
Simulation parameters. Region names refer to Fig. 2.

Physical parameters		
Electrolyte/Neuron (Custom Semiconductor)	ε_r	80
	E_g	0 eV
	N_c= N_v	N_{av} $c_{i/e}$ cm^{-3}
	μ_n=μ_p	$4 \cdot 10^{-4}$ cm^2/Vs
Membrane (Insulator)	ε_r	11.7
p-doped Si	N_A	$5 \cdot 10^{17}$ cm^{-3}
n-doped Si	N_D	$1 \cdot 10^{19}$ cm^{-3}
n^+-doped Si	N_D	$1 \cdot 10^{20}$ cm^{-3}
Geometrical parameters		
Intrinsic neuron surface	A_{int}	0.15 µm^2
Extrinsic neuron surface	A_{ext}	219.85 µm^2

N_{av} is the Avogadro's number.
$c_{i/e}$ is the molar concentration in the intra/extra-cellular fluids.

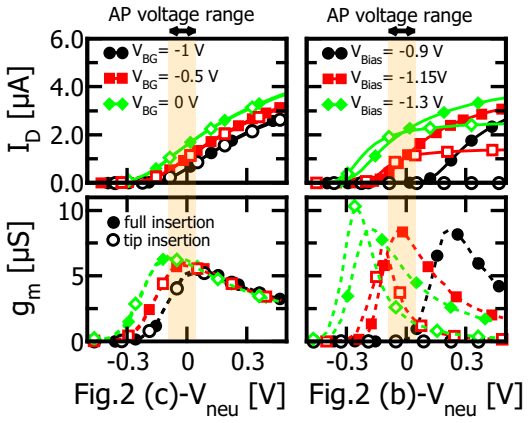

Fig. 3. I_D (top panels) and g_m (bottom panels) versus intracellular potential V_{neu} for the EG-SOI-FET (left panels) with the extended-gate *fully coated* with lateral oxide (Fig. 2 c) and for the VNW-FET (right panels) with the NW *partially coated* with lateral oxide (Fig. 2 b), both in tip and full insertion into neuron. The intracellular potential, V_{neu}, works as the conventional V_{GS} of MOSFETs. V_{BG} is applied to the back-gate (BG) of the EG-SOI-FET (left panels) and V_{Bias} to the source, drain, bulk of the VNE-FET, to adjust their threshold voltage and thus maximize their transconductance in the AP voltage range (shaded orange-box). V_{DS} = 50 mV.

(Fig. 2 a, b); 2) a back-gate voltage V_{BG} to the EG-SOI-FET back gate (Fig. 2 c, d).

Fig. 3 shows the V_T shift for changes of V_{BG} on device (c) in Fig. 2 (left panels), and for changes of V_{bias} on device (b) in Fig. 2 (right panels) for tip and full insertion conditions. The curves for the *fully coated* EG-SOI-FET are well behaved (typical of a FET with linear I_D vs V_{GS}), while those for the *partially coated* VNW-FET flatten out rapidly above threshold, mostly due to the large series resistance of the vertical S/D. On the whole, for proper DC bias values (see red curves in Fig. 3), $g_{m,MAX}$ shifts to the $V_{neu,m}$. Similar results have been obtained for structures (a) and (d) as well (not shown for brevity).

Tab. II lists the optimized bias points, I_{D0}=I_D($V_{neu,rest}$) where $V_{neu,rest}$=-70 mV is the resting membrane potential, and $g_{m,MAX}$=g_m($V_{neu,m}$), for all configurations and insertion conditions in Fig. 2. The fully coated VNW-FET (Fig. 2 a) has the highest $g_{m,MAX}$ for all insertion conditions. Despite the larger coupling surface of the partially coated VNW-FET (Fig. 2 b) compared to the fully coated one for full insertion, the former has lower $g_{m,MAX}$ because of the longer channel; this result is exacerbated in tip insertion by a reduced coupling area with the intracellular medium.

TABLE II
OPTIMUM BIAS POINTS FOR SENSING AT V_{DS}=50 mV

Structure & insertion type	DC bias [V]	I_{D0} [µA]	$g_{m,MAX}$ [µS]
Fig. 2 (a) - full	V_{bias}=−1.05	0.23	14.21
Fig. 2 (a) - tip	V_{bias}=−1.05	0.23	14.07
Fig. 2 (b) - full	V_{bias}=−1.15	0.50	8.55
Fig. 2 (b) - tip	V_{bias}=−1.15	0.78	3.46
Fig. 2 (c) - full	V_{BG}=−0.5	0.61	5.99
Fig. 2 (c) - tip	V_{BG}=−0.5	0.61	5.91
Fig. 2 (d) - full	V_{BG}=0.0	1.10	6.65
Fig. 2 (d) - tip	V_{BG}=0.0	1.44	2.13

Similarly to the fully coated VNW-FET, the EG-SOI-FET (Fig. 2 c) is essentially insensitive to the insertion type. However, it achieves a lower $g_{m,MAX}$ because of the longer channel and of the less efficient gate-oxide/channel-coupling (the channel of the former is directly coupled by the EDL in the electrolyte, whereas the latter one undergoes a capacitive divider between the same EDL and the gate-oxide of the SOI-FET). Lastly, the partially coated EG-SOI-FET (Fig. 2 d) delivers a larger $g_{m,MAX}$ than the fully coated version because of a larger cell surface coupled to the nanoelectrode in full insertion. However, this pro becomes a drawback for tip insertion conditions, as the gate couples strongly to the grounded extracellular fluid.

B. Transient response to an action potential

We now examine the transient response to an action potential (AP) for the previously identified optimum biases. Fig. 4 shows how the intracellular potential $V_{neu}(t)$ during an AP (top panel) is transduced into $I_D(t)$ (middle and bottom panels) by the devices in Fig. 2 for tip and full insertion. The AP is generated by the two-compartments HH circuit stimulated by a single current-pulse (110 pA, 0.5 ms in duration, not shown in Fig. 4), to avoid that a constant stimulus spoils the recorded signal [16].

Fig. 4 also shows that the DC bias of the FET does not affect the AP generation mechanism, as all the $V_{neu}(t)$ are identical. This is observed only if the distributed nature of the neuron firing is captured with at least two HH compartments. In fact, we verified that unphysical behaviors of the firing neuron emerge for partially coated nanoelectrodes with a one compartment model. Indeed, the large extrinsic HH compartment that describes the portion of the neuron outside the simulation domain strongly mitigates the parasitic coupling of the device to the intracellular medium.

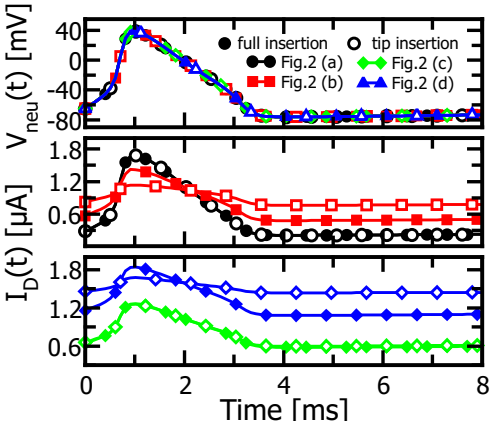

Fig. 4. Transient response to an AP recorded by the VNW-FET of Fig. 2 (a, b) and by the EG-SOI-VNW-FET of Fig. 2 (c, d) for tip and full insertion conditions. The AP is generated by a two-compartments HH circuit stimulated by a single current-pulse (see main text). DC bias values as in Tab. II.

Furthermore, fully coated structures yield the same current waveform regardless of the nanoelectrode insertion depth (black and green curves). Partially coated ones, instead, exhibit differences in spite of the larger neuron/electrode coupling area. To mitigate the coupling variability fully coated structures are therefore preferable.

C. Neuron-to-device transfer function

To corroborate the proposed approach to set the maximum g_m in the AP voltage range, we extend the analysis to the frequency domain. The neuron-to-device transfer function, $|H(f)| = |I_D(f)/V_{neu}(f)|$, has been computed by small-signal AC simulations of all structures, configurations and insertions over the frequency range of AP spectrum ($\approx$ 1 mHz $\div$ 10 kHz). As the readout circuit is not included in the simulation, there is no evidence of zeros or poles, and the $|H(f)|$ are essentially flat (not shown). $|H(f)|$ is thus expected to be close to the g_m (DC value). This observation is confirmed by Fig. 5 where $|H(f)|$ at 1 kHz is compared to the maximum transconductance $g_{m,MAX}$ in Tab. II.

V. Conclusions

We extended the numerical model for neuron/device coupling of [7] implementing via the SDevice CMIs an accurate compartmental description of the neuron membrane with HH models. For both VNW-FET and EG-SOI-FET designs, a partial nanoelectrode coating makes the transduction gain dependent on the insertion depth, resulting in unpredictable signal amplitudes. Therefore, a full nanoelectrode coating is preferable for both architectures. Compartmentalization of the membrane is key to avoid unphysical model predictions; if multiple compartments are adopted, then the model suggests that a full nanoelectrode lateral coating is preferable for stable recordings in spite of a reduced coupling area.

In terms of performance, the VNW-FET achieves a higher transconductance w.r.t. to the EG-SOI-FET at the expense of a larger optimum DC bias. Even if such bias does not seem to affect the natural AP genesis (see Fig.4), its biocompatibility with neurons' physiology should be examined carefully.

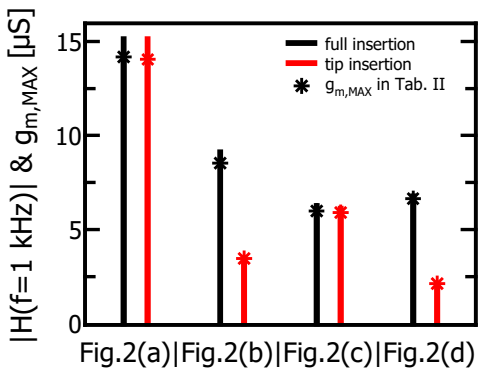

Fig. 5. Comparison between the neuron-to-device transfer-function $|H(f)| = |I_D(f)/V_{neu}(f)|$ at f=1 kHz (solid lines) and the $g_{m,MAX}$ of Tab. II ($*$ symbols). DC bias values as in Tab. II. $|H(f)|$ is approximately constant in the frequency range of the AP spectrum (not shown).

Acknowledgment

The authors acknowledge useful technical discussions with all the partners of the H2020 EC project "IN-FET".

References

[1] Y. Wu, H. Chen, and L. Guo, "Opportunities and dilemmas of in vitro nano neural electrodes," *RSC Advances.*, vol. 10, pp. 187–200, 2020. 10.1039/C9RA08917A.

[2] S. Vassanelli and M. Mahmud, "Trends and challenges in neuroengineering: Toward "intelligent" neuroprostheses through brain-"brain inspired systems" communication," *Frontiers in Neuroscience*, vol. 10, 2016. 10.3389/fnins.2016.00438.

[3] M. E. Spira and A. Hai, "Multi-electrode array technologies for neuroscience and cardiology," *Nature nanotechnology*, vol. 8, no. 2, pp. 83–94, 2013. 10.1038/nnano.2012.265.

[4] G. He, N. Hu, A. M. Xu, X. Li, Y. Zhao, and X. Xie, "Nanoneedle platforms: The many ways to pierce the cell membrane," *Advanced Functional Materials*, vol. 30, no. 21, p. 1909890, 2020. 10.1002/adfm.201909890.

[5] Synopsys, Inc., Sentaurus Device v. N-2017.09.

[6] Comsol, Inc., Comsol Multiphysics v. 6.0.

[7] F. Leva, P. Palestri, , and L. Selmi, "Multiscale simulation analysis of passive and active micro/nano-electrodes for cmos-based in-vitro neural sensing devices," *Philosophical Transactions of the Royal Society A: Mathematical, Physical and Engineering Sciences*, in press. 10.1098/rsta.2021.0013.

[8] I.-Y. Chung, H. Jang, J. Lee, H. Moon, S. M. Seo, and D. H. Kim, "Simulation study on discrete charge effects of sinw biosensors according to bound target position using a 3d tcad simulator," *Nanotechnology*, vol. 23, no. 6, p. 065202, 2012. doi:10.1088/0957-4484/23/6/065202.

[9] A. Bandiziol, P. Palestri, F. Pittino, D. Esseni, and L. Selmi, "A tcad-based methodology to model the site-binding charge at isfet/electrolyte interfaces," *IEEE Transactions on Electron Devices*, vol. 62, no. 10, pp. 3379–3386, 2015. doi:10.1109/TED.2015.2464251.

[10] J. J. Harris, R. Jolivet, E. Engl, and D. Attwell, "Energy-efficient information transfer by visual pathway synapses," *Current Biology*, vol. 25, no. 24, pp. 3151–3160, 2015. doi:10.1016/j.cub.2015.10.063.

[11] L. Chua, "Device modeling via nonlinear circuit elements," *IEEE Transactions on Circuits and Systems*, vol. 27, no. 11, pp. 1014–1044, 1980. doi:10.1088/0957-4484/23/6/065202.

[12] M. Parodi and M. Storace, "On a circuit representation of the hodgkin and huxley nerve axon membrane equations," *International journal of circuit theory and applications*, vol. 25, no. 2, pp. 115–124, 1997. doi: 10.1002/(SICI)1097-007X(199703/04)25:2¡115::AID-CTA957¿3.0.CO;2-#.

[13] D. Biolek, V. Biolkova, and Z. Kolka, "Spice models of memristive devices forming a model of hodgkin-huxley axon," in *2013 18th International Conference on Digital Signal Processing (DSP)*, pp. 1–5, IEEE, 2013. doi:10.1109/ICDSP.2013.6622743.

[14] A. L. Hodgkin and A. F. Huxley, "A quantitative description of membrane current and its application to conduction and excitation in nerve," *The Journal of physiology*, vol. 117, no. 4, p. 500, 1952. doi: 10.1113/jphysiol.1952.sp004764.

[15] S. Martinoia, P. Massobrio, M. Bove, and G. Massobrio, "Cultured neurons coupled to microelectrode arrays: circuit models, simulations and experimental data," *IEEE Transaction on Biomedical Engineering*, vol. 51, no. 5, pp. 859–863, 2004. doi: 10.1109/TBME.2004.826607.

[16] G. Massobrio, S. Martinoia, and P. Massobrio, "Equivalent circuit of the neuro-electronic junction for signal recordings from planar and engulfed micro-nano-electrodes," *IEEE Transactions on Biomedical Circuits and Systems*, vol. 12, no. 1, pp. 3–12, 2018. doi: 10.1109/TBCAS.2017.2749451.

[17] S. M. Ojovan, N. Rabieh, N. Shmoel, H. Erez, E. Maydan, A. Cohen, and M. E. Spira, "A feasibility study of multi-site, intracellular recordings from mammalian neurons by extracellular gold mushroom-shaped microelectrodes," *Scientific reports*, vol. 5, no. 1, pp. 1–14, 2015. 10.1038/srep14100.